BENHA MEDICAL JOURNAL bmj

Print ISSN 1110-208X.

Online ISSN 2357-0016

The Possible Protective Role of Avocado Oil on the Chlorpyrifos Pesticide Induced Thyroid Injury in Adult Male Albino Rats. (Light, Electron Microscopic and Immunohistochemical Studies)

Nehal H. Mostafa , Essam M. Eid, Ali M. Ali, Marim F. Abdow

Anatomy and Embryology Department, Faculty of Medicine Benha University, Egypt.

Corresponding to:
Dr. Nehal H. Mostafa.
Anatomy and Embryology Department, Faculty of Medicine Benha University, Egypt.
Email: nehal.hossam@fmed.bu.edu.eg

Received:6 October 2025
Accepted:10 November 2025

Abstract:

Background: Chlorpyrifos (CPF), an organophosphorus pesticide, negatively affects the thyroid gland, while avocado oil possesses antioxidant properties that may offer protection. Aim: The present study aimed to evaluate the protective role of avocado oil against CPF-induced thyroid toxicity in adult male albino rats. **Methods:** 40 adult male albino rats were randomly divided into four groups (n = 10 each); the control group (G I) received no treatment, the avocado-treated group (G II) received avocado oil at 4 ml/kg body weight/day orally once daily for six weeks, the CPF group (G III) was administered CPF at 6.7 mg/kg body weight/day, dissolved in 4 ml/kg corn oil, orally once daily for six weeks, and the avocado + CPF group (G IV) received both avocado oil and CPF at the same doses and duration as G II and G III. **Results:** CPF caused marked disruption of thyroid histological architecture, reduced PAS-positive reaction, increased caspase-3 immuno-expression, and severe ultrastructural alterations in follicular and parafollicular cells. Co-administration of avocado oil with CPF largely restored normal histological appearance, enhanced PAS reactivity, decreased caspase-3 immuno-expression, and improved ultrastructural integrity of follicular and parafollicular cells. **Conclusion:** Avocado oil exerts a potent protective effect against CPF-induced thyroid damage, mitigating histological, histochemical, immunohistochemical, and ultrastructural alterations.

Keywords: Chlorpyrifos; Thyroid; Avocado oil and caspase 3.

Introduction

The thyroid gland and its hormones are fundamental for numerous biological processes in both pediatric and adult populations, playing a central role in growth, metabolic regulation, and overall development [1,2,3].

The widespread agricultural application of CPF leads to its dispersion into multiple environmental compartments, including air, soil, and water, thereby increasing the potential for human and animal exposure [4]. Additionally, residues of CPF have been consistently detected in fruits, grains, and vegetables, raising concerns regarding dietary exposure [5]. Mechanistically, CPF induces the generation of reactive oxygen species (ROS) and triggers oxidative stress, which can disrupt normal cellular differentiation and impair physiological functions [6].

Avocado (Persea americana) is a tropical and subtropical fruit notable for its lipid-rich pulp, which makes it a highly suitable source for oil extraction [7][8]. The growing popularity of avocado oil is largely attributed to its high content of health-promoting unsaturated fatty acids, particularly monounsaturated fatty acids (MUFAs), as well as multiple bioactive compounds such as carotenoids, vitamins (including E and B-complex), and tocopherols [9][10].Beyond its intrinsic antioxidant properties, avocado consumption has been shown to enhance the absorption of antioxidants from other dietary sources [11]. The major antioxidant constituents identified in avocado oil include β-sitosterol, tocopherol, γ-tocopherol, campesterol, stigmasterol, sitostanol, and campestanol, which collectively contribute to its protective biological effects [7].

Materials and methods

Animals

The present study involved 40 healthy adult male albino rats, weighing between 180–220 g and aged 10–12 weeks. Animals were procured from the Holding Company for Biological Products and Vaccines (Vacsera), Helwan, Egypt, and housed in the Experimental Animal Unit, Faculty of Medicine, Benha University. The experimental period extended from July 5, 2023, to August 20, 2023. Rats were maintained in specialized cages with three animals per cage at room temperature, provided with unrestricted access to tap water and standard commercial diet, and subjected to a 12-hour light/dark cycle. All procedures were conducted in accordance with the guidelines approved by the Research Ethical Committee of the Faculty of Medicine, Benha University {M.S. 17-3-2023}.

Materials

CPF was obtained from ICTA Company, Giza, Egypt, as ICTAfos EC 48% and administered at a dose of 6.7 mg/kg/day. CPF was prepared by dissolving it in corn oil at a concentration of 4 ml/kg/day [12]. Specifically, 1 ml of CPF solution was diluted in 71.5 ml of corn oil, resulting in a solution where 1 ml contained 6.7 mg CPF. Accordingly, each rat, weighing approximately 200 g, received 0.2 ml of this solution daily, corresponding to 1.34 mg CPF per day. Avocado oil was purchased from EL Hawag Company for Extraction and Packing of Natural Oils, Cairo, Egypt, and administered at a dose of 4 ml/kg/day [13].

Experimental Design

Rats were randomly divided into four equal groups, with 10 animals per group:

- **Group I (Control group):** subdivided into:
  - **Subgroup Ia:** Five rats maintained without treatment for six weeks.
  - **Subgroup Ib:** Five rats received corn oil (vehicle for CPF) at 4 ml/kg/day orally via gastric tube, five days per week, for six weeks.
- **Group II (Avocado oil-treated group):** 10 rats were given avocado oil at 4 ml/kg/day orally via gastric tube, five days per week, for six weeks.

- **Group III (CPF-treated group):** 10 rats were administered CPF at 6.7 mg/kg/day dissolved in 4 ml/kg corn oil orally via gastric tube, five days per week, for six weeks.
- **Group IV (CPF + avocado oil-treated group):** 10 rats received both CPF and avocado oil concurrently at the same doses and durations as Groups II and III.

Sample Collection

At the end of the six-week experimental period, rats were anesthetized using diethyl ether inhalation and sacrificed via cervical dislocation. Thyroid glands were carefully dissected and excised through cervical incisions to ensure complete removal and preserve tissue integrity for subsequent analyses.

Histopathological study:

Hematoxylin/Eosin, PAS, and Caspase-3 immunostaining were used to prepare 5 μm thick sections of thyroid paraffin for light microscopic analysis after fixation in 10% formaldehyde.

Electron microscopic study:

Transmission electron microscope (TEM) was used for ultrastructural examination of the thyroid gland after immediate fixation in 4% glutaraldehyde.

Morphometric study:

Immunoassay photomicrographs, to evaluate means areas percentages of PAS positive reaction and Caspase-3 immuno-expression at magnification x400.

Statistical study:

Data, obtained from the morphometric study, were collected, arranged and then analyzed using statistical package of social sciences (SPSS) version 20 (IBM SPSS Statistics for Windows, Armonk, NY, USA). The results were expressed as mean ± SD for each group. One-way analysis of variance (ANOVA) test was conducted to detect P value: if >0.05 it was considered statistically non-significant. P-value of≤0.05 it was considered statistically significant. P-value of≤0.001 it was considered statistically highly significant.

Histological Results

H&E Findings:

- **Group I and II:** Thyroid sections demonstrated preserved normal architecture with numerous follicles of variable sizes and shapes. Follicles were lined by a single layer of follicular cells; some cells were cuboidal with rounded nuclei, while others were flattened with oval nuclei. Follicular cells rested upon a thin basement membrane. Follicular lumens contained homogeneous acidophilic colloid. Parafollicular cells appeared as larger, pale cells arranged in clusters between follicles. Follicles were separated by thin connective tissue septa containing elongated fibroblasts and blood capillaries (Figs. 1a–f).
- **Group III:** Sections showed disruption of normal thyroid follicular architecture. Some follicles displayed discontinuity in the lining epithelium and fusion of adjacent follicles. Certain follicles exhibited desquamation of follicular cells into the lumen with degeneration of some epithelial cells. Follicular cells showed vacuolated cytoplasm and pyknotic nuclei. Other follicles demonstrated hyperplasia of follicular cells. Several follicles exhibited absent or reduced colloid. Parafollicular cells appeared clustered and showed hyperplasia. An increase in interfollicular connective tissue with dilated, congested capillaries was noted (Figs. 2a–c).
- **Group IV:** Sections revealed partial restoration of normal thyroid histology. Follicles varied in size and shape, with many appearing nearly normal, containing acidophilic colloid and lined with cuboidal or flat follicular cells with regular nuclei. However, a few follicles showed discontinuity in the epithelial lining, fusion, desquamation, and reduced colloid. Parafollicular cells were clustered with mild hyperplasia. Follicles were separated by thin connective tissue (Figs. 2d–f).

PAS Findings:

- **Group I and II:** Strong PAS positivity was observed in the follicular colloid as well as within the basement membrane.
- **Group III:** Weak PAS staining was evident in the colloid, with some follicles entirely devoid of colloid. The distorted basement membrane of follicles exhibited weak PAS reaction.
- **Group IV:** Moderate PAS staining was detected in the colloid, with weak positivity in the follicular basement membrane (Figs. 3a–d).

Caspase-3 Immunohistochemistry:

- **Group I and II:** Follicular cells demonstrated negative nuclear and cytoplasmic immunoreactivity for caspase-3.
- **Group III:** Strong positive nuclear and cytoplasmic staining for caspase-3 was observed in many follicular cells.
- **Group IV:** Mixed reactivity was noted, with some follicular cells negative and others positive for nuclear and cytoplasmic caspase-3 immunostaining (Figs. 4a–d).

Electron Microscopy Findings:

- **Group I and II:** Follicular epithelial cells exhibited apical microvilli projecting into the colloid, distinct cell membranes, and intact apical junctional complexes. Nuclei were heterochromatic with well-formed nuclear membranes. Cytoplasm contained rough endoplasmic reticulum (rER) cisternae, electron-dense elongated mitochondria, apical lysosomes, and colloid droplets. Follicular cells rested on an intact basement membrane. Parafollicular cells were located within the basement membrane, with oval heterochromatic nuclei and cytoplasm containing small electron-dense secretory vesicles (Figs. 5a, c and 6a).
- **Group III:** Follicular epithelial cells were fused with distorted apical microvilli. Nuclei were heterochromatic with irregular membranes and shrinkage. Cytoplasm showed dilated, disrupted rER, degenerated mitochondria, and electron-dense lysosomes. Follicular basement membranes were distorted. Parafollicular cells exhibited heterochromatic nuclei with irregular nuclear membranes and multiple cytoplasmic vacuoles (Figs. 5b and 6b).
- **Group IV:** Follicular epithelial cells displayed apical microvilli projecting into the colloid with widened intercellular spaces. Nuclei were euchromatic with distinct nuclear membranes. Cytoplasm contained dilated rER and apical electron-dense lysosomes. Parafollicular cells lay adjacent to follicles, with euchromatic nuclei and peripheral heterochromatin, intact nuclear membranes, and cytoplasm containing small electron-dense secretory vesicles and rER cisternae (Figs. 5d and 6c).

Morphometric and Statistical Results:

- **PAS-positive Colloid Area (%) (Table 1):**

Significant differences were observed among groups. **Group I** had a mean area of 93.72 ± 1.21, significantly higher than all groups except **Group II**. **Group III** showed the lowest mean (34.87 ± 5.83), differing significantly from all other groups. **Group II** exhibited a mean of 94.88 ± 1.84, significantly differing from **Groups III** and **IV** (77.22 ± 4.97).

- **Caspase-3 Positive Area (%) (Table 2):**

Significant differences were observed between groups. **Group I** had a mean of 5.33 ± 1.52, significantly lower than all groups except **Group II**. **Group III** had the highest mean (69.03 ± 3.86), significantly differing from all other groups. **Group II** exhibited a mean of 4.82 ± 0.78, significantly lower than **Groups III** and **IV**.

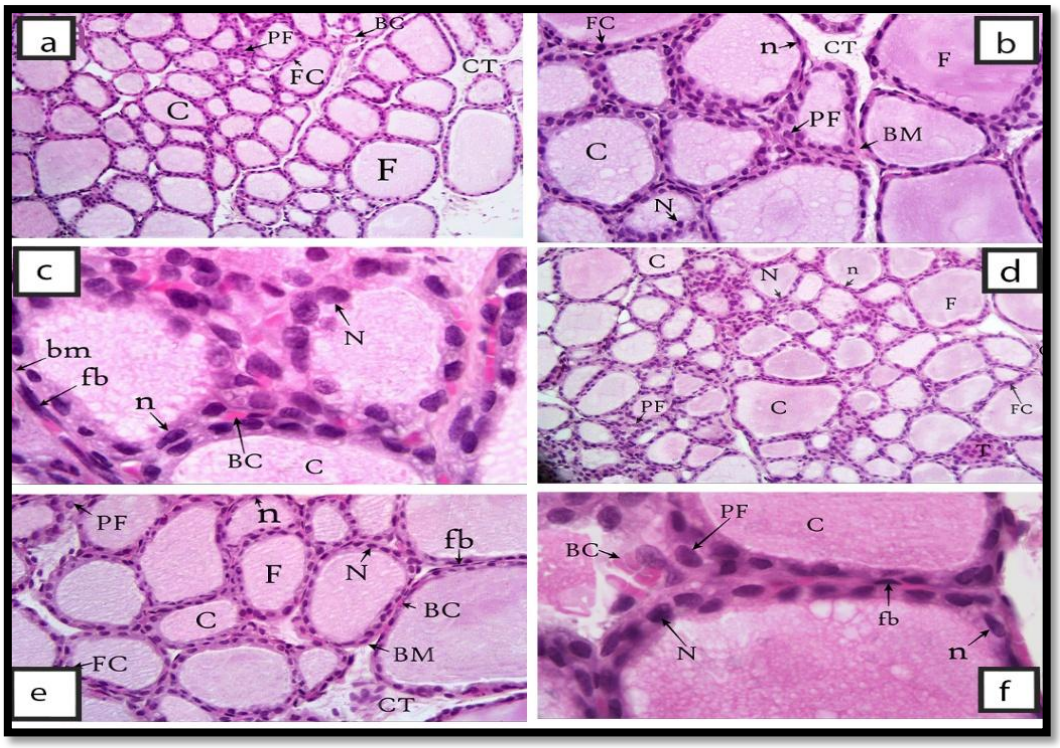

Figure 1: A photomicrograph of thyroid gland sections from control (G I) and avocado-treated (G II) rats.

(a) Thyroid section of a control rat (G I) showing normal architecture with numerous thyroid follicles (F) of variable sizes and shapes, lined by a single layer of follicular cells (FC). Follicular lumina contain homogenous acidophilic colloid (C). Parafollicular cells (PF) appear in clusters between follicles. Follicles are separated by thin connective tissue (CT) containing blood capillaries (BC). (H&E ×200)

(b) Control group (G I) showing thyroid follicles (F) lined by follicular cells (FC); some cuboidal with rounded nuclei (N), others flat with oval nuclei (n), resting on a thin basement membrane (BM). Lumen contains acidophilic colloid (C). Parafollicular cells (PF) clusters between follicles, which are separated by thin CT can be seen. (H&E ×400)

(c) High magnification of control thyroid (G I) displaying follicles separated by thin CT septa containing fibroblast cells (fb) and BC. Follicular cells which vary from cuboidal cells with rounded nuclei (N) to flat cells with flat nuclei (n), resting on basement membrane (bm) are noticed. Lumina appear filled with acidophilic colloid (C). (H&E oil ×1000)

(d) Thyroid of avocado-treated rat (G II) showing normal architecture, follicles (F) of variable sizes lined with FC; cuboidal cells with rounded nuclei (N) and flat cells with oval nuclei (n). PF cells clusters between follicles, lumina filled with acidophilic colloid (C), follicles separated by thin CT. Tangential mass (T) of follicular epithelial cells observed. (H&E ×200)

(e) Higher magnification of G II showing follicles (F) lined with FC; cuboidal (N) and flat (n), with intact basement membrane (bm). Lumina filled with colloid (C) are noticed. PF cells in clusters with CT in between containing fibroblasts (fb) and BC are seen. (H&E ×400)

(f) High magnification of G II showing follicular lumina filled with colloid (C), lined by follicular cells ranging from squamous (n) to cuboidal (N). Follicles separated by thin CT containing fibroblasts (fb) and BC are observed. (H&E oil ×1000)

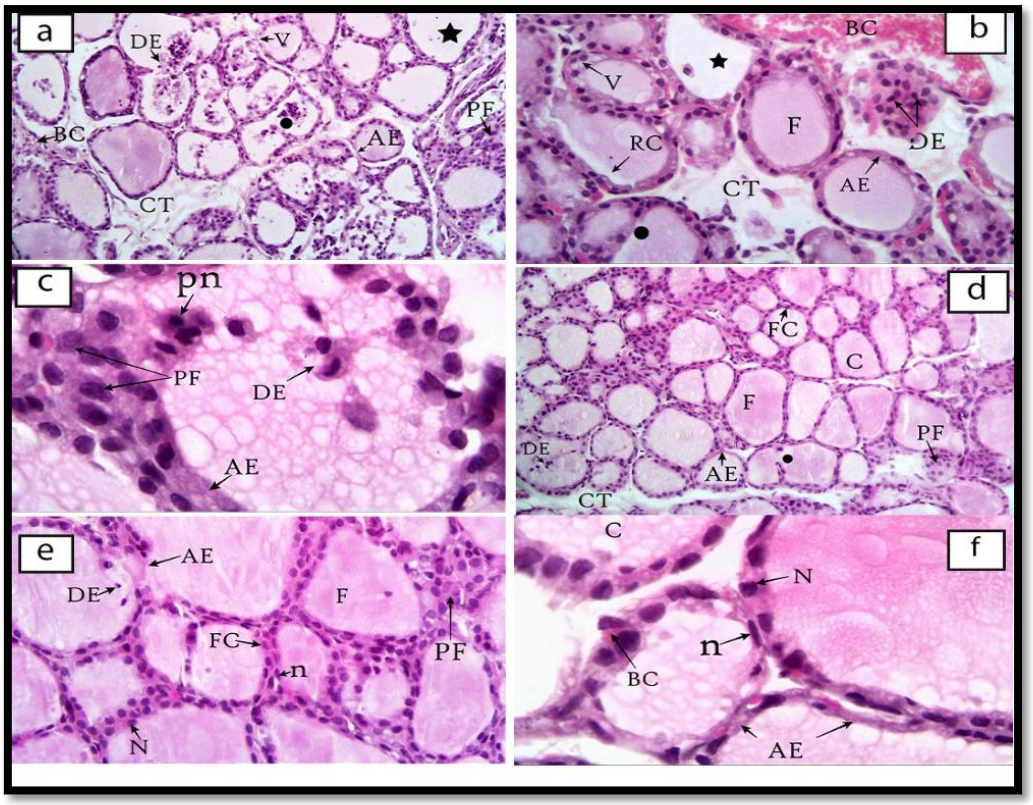

Figure 2: A photomicrograph of thyroid gland sections from CPF-treated (G III) and avocado + CPF-treated (G IV) rats.

(a) Thyroid section of CPF-treated rat (G III) showing disrupted follicular architecture. Some follicles exhibit epithelial discontinuity and fusion (dot). Parafollicular cells (PF) are hyperplastic. Follicular cells show desquamation (DE), vacuolated cytoplasm (V), and degeneration (AE). Some follicles lack colloid (star). Interfollicular connective tissue (CT) is seen expanded with blood capillaries (BC). (H&E ×200)

(b) CPF-treated thyroid section (G III) showing disrupted follicles (F) with degenerated epithelial cells (AE), vacuolated cytoplasm (V), reduced colloid (RC) or absent colloid (star), hyperplastic PF, and expanded CT with dilated congested BC. (H&E ×400)

(c) High magnification of G III section showing degenerated epithelial cells (AE), pyknotic nuclei (pn), desquamated cells (DE) in lumina, and hyperplastic PF clusters. (H&E oil ×1000)

(d) Thyroid section of avocado + CPF-treated rat (G IV) showing follicles (F) of variable sizes and shapes. Some follicles appear nearly normal with acidophilic colloid (C), while others contain degenerated cells (AE), desquamated cells (DE), reduced colloid (RC), or fused epithelium (dot). PF clusters show mild hyperplasia. Follicles are seen separated by thin CT. (H&E ×200)

(e) G IV section showing follicles with nearly normal lining epithelium; cuboidal cells with rounded nuclei (N) or flat cells with oval nuclei (n), some degenerated cells (AE), few desquamated cells (DE), and PF clusters with hyperplasia. (H&E ×400)

(f) High magnification of G IV section showing nearly normal follicles filled with colloid (C), follicles lined with cuboidal (N) or flat (n) cells, while some show degenerated epithelial cells (AE). Follicles are seen separated by thin CT septa with BC. (H&E oil ×1000)

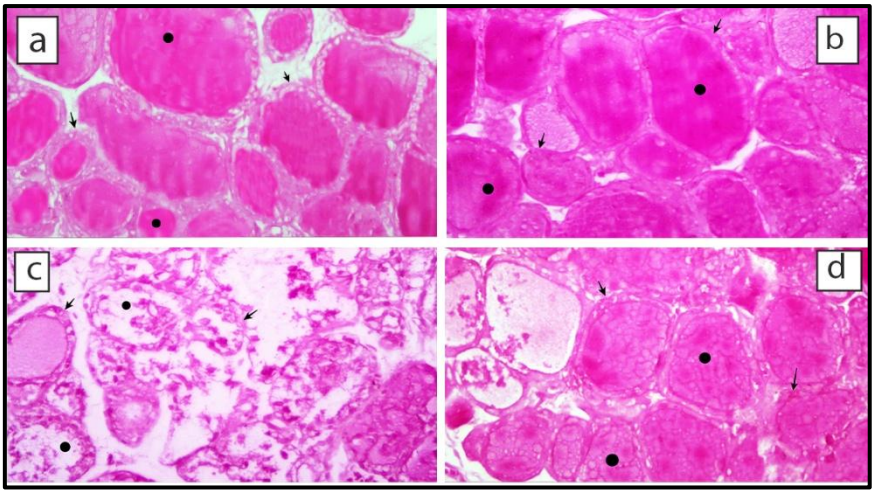

Figure 3: A photomicrograph of thyroid gland sections showing PAS staining in control, CPF-treated, avocado-treated, and avocado + CPF-treated rats.
(a) Control group (G I) section displaying strong PAS reaction in colloids (circles) and strong PAS positivity in follicular basement membranes (arrows). (PAS ×400)
(b) Avocado-treated group (G II) section demonstrating strong PAS reaction in colloids (circles) and strong PAS positivity in follicular basement membranes (arrows). (PAS ×400)
(c) CPF-treated group (G III) section showing weak PAS reaction in colloids, with some follicles completely empty (circles), and attenuated PAS staining in distorted follicular basement membranes (arrows). (PAS ×400)
(d) Avocado + CPF-treated group (G IV) section exhibiting moderate PAS reaction in colloids (circles) and weak PAS positivity in follicular basement membranes (arrows). (PAS ×400)

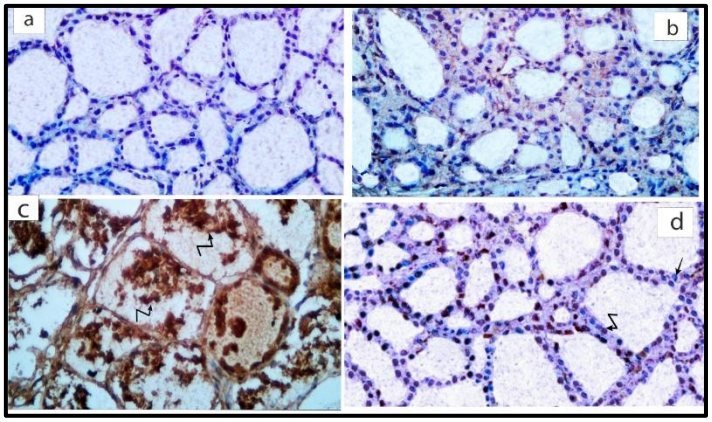

Figure 4: A photomicrograph of thyroid gland sections showing caspase-3 immunostaining in control, CPF-treated, avocado-treated, and avocado + CPF-treated rats.
(a) Control group (G I) section exhibiting negative nuclear and/or cytoplasmic immunoreactivity for caspase-3 in follicular cells. (Caspase-3 immunostaining ×400)
(b) Avocado-treated group (G II) section demonstrating negative nuclear and/or cytoplasmic immunoreactivity for caspase-3 in follicular cells. (Caspase-3 immunostaining ×400)
(c) CPF-treated group (G III) section showing strong positive nuclear and/or cytoplasmic immunoreactivity for caspase-3 in numerous follicular cells (zigzag arrow). (Caspase-3 immunostaining ×400)
(d) Avocado + CPF-treated group (G IV) section showing mixed immunoreactivity: some follicular cells are negative (straight arrow), while others are positive (zigzag arrow) for nuclear and/or cytoplasmic caspase-3. (Caspase-3 immunostaining ×400)

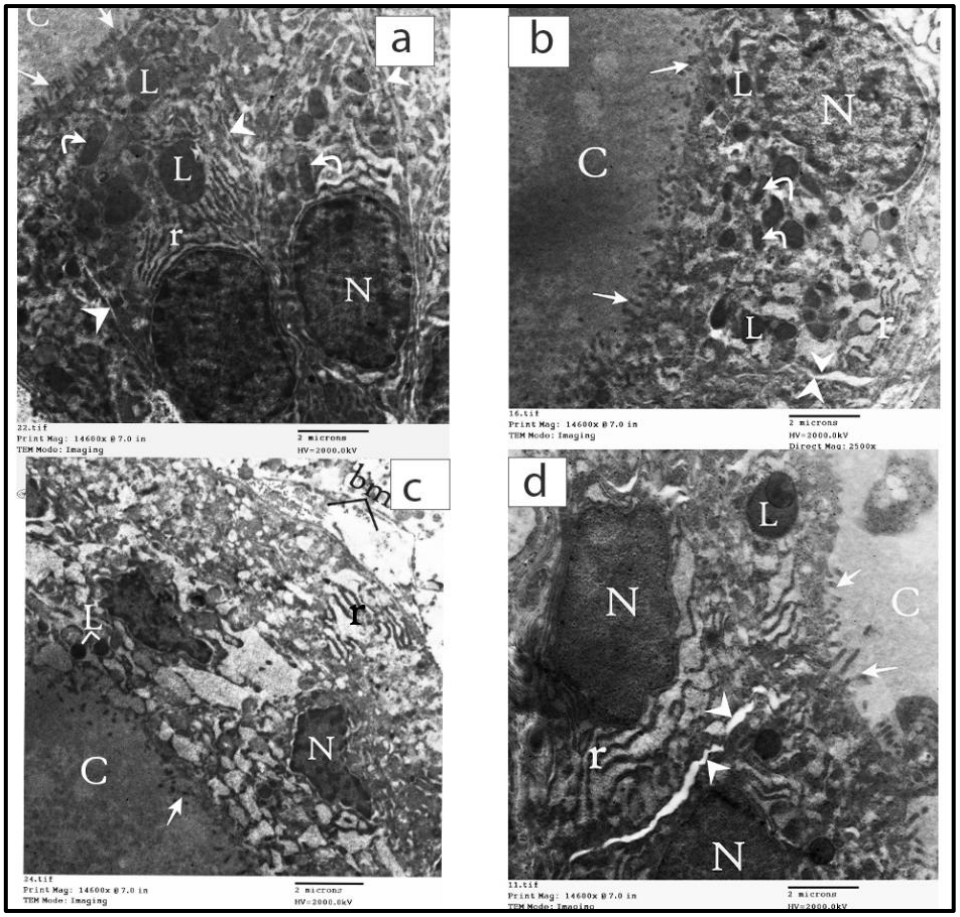

Figure 5: A transmission electron micrograph of thyroid gland ultrathin sections from control, CPF-treated, avocado-treated, and avocado + CPF-treated rats.
(a) Control group (G I) section showing adjacent follicular epithelial cells with apical microvilli (arrow) projecting into the colloid (C), distinct cell membranes (arrowhead) between cells, heterochromatic nuclei (N) with regular nuclear membrane. Cytoplasm containing rough endoplasmic reticulum cisternae (r), electron-dense elongated mitochondria (curved arrow), and apical electron-dense lysosomes (L) can be seen. (TEM ×14,600)
(b) Avocado-treated group (G II) section displaying follicular epithelial cells with apical microvilli (arrow) projecting into colloid (C), distinct cell membranes (arrowhead), euchromatic nuclei (N) with peripheral heterochromatic condensation. Cytoplasm containing rough endoplasmic reticulum cisternae (r), elongated electron-dense mitochondria (curved arrow), and apical electron-dense lysosomes (L) can be observed. (TEM ×14,600)
(c) CPF-treated group (G III) section showing fused follicular epithelial cells with distorted apical microvilli (arrow), shrunken heterochromatic nuclei (N) with irregular nuclear membrane. Cytoplasm containing dilated and destructed rough endoplasmic reticulum cisternae (r) and electron-dense lysosomes (L), and distorted basement membrane (bm) can be seen. (TEM ×14,600)
(d) Avocado + CPF-treated group (G IV) section showing follicular epithelial cells with apical microvilli (arrow), wide space between adjacent cell membranes (arrowhead), euchromatic nuclei (N) with distinct nuclear membrane. Cytoplasm containing dilated rough endoplasmic reticulum (r) and apical electron-dense lysosomes (L) can be seen. (TEM ×14,600)

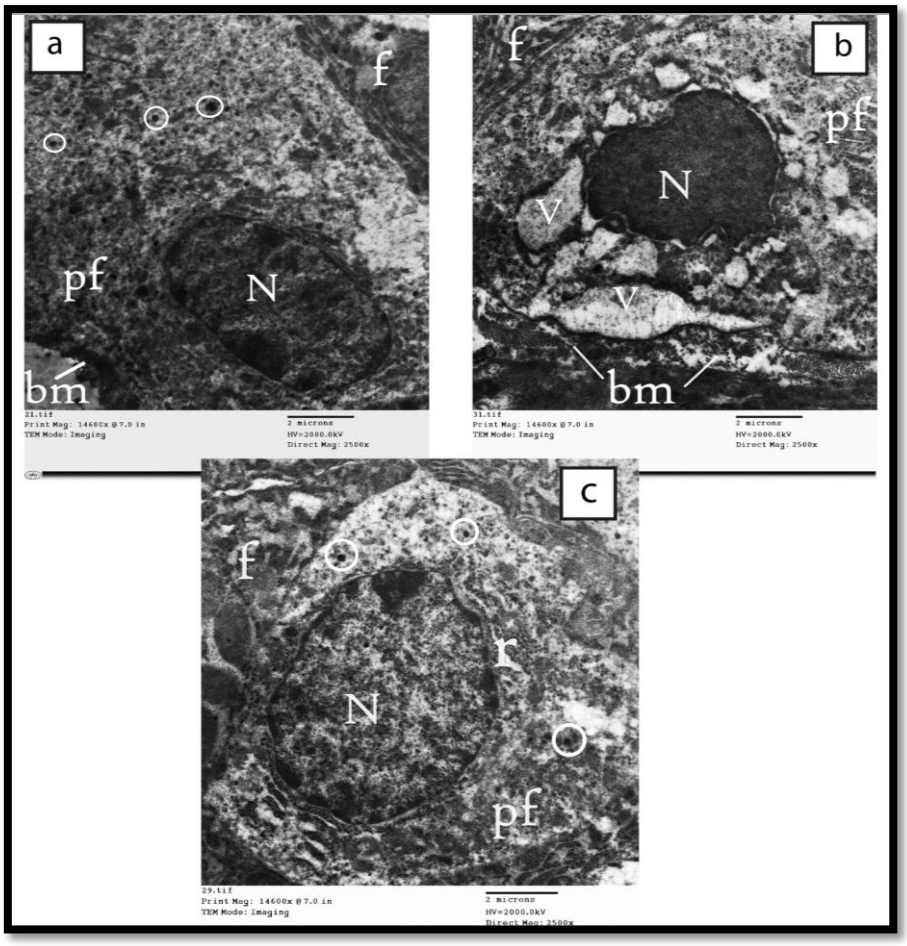

Figure 6: A transmission electron micrograph of parafollicular cells in thyroid gland ultrathin sections from control, CPF-treated, and avocado + CPF-treated rats.
(a) Control group (G I) showing parafollicular cell (pf) located within the basement membrane (bm) of follicular cell (f), with oval heterochromatic nucleus (N) and regular nuclear membrane. Cytoplasm contains multiple small electron-dense secretory vesicles (circle). (TEM ×14,600)
(b) CPF-treated group (G III) showing parafollicular cell (pf) within the basement membrane of follicular cell (f), with heterochromatic nucleus (N) and irregular nuclear membrane. Cytoplasm contains multiple vacuoles (V). (TEM ×14,600)
(c) Avocado + CPF-treated group (G IV) showing parafollicular cell (pf) adjacent to follicular cell (f), with euchromatic nucleus (N), peripheral heterochromatic condensation, regular nuclear membrane, and cytoplasm containing multiple small electron-dense secretory vesicles (circle) and rough endoplasmic reticulum cisternae (r). (TEM ×14,600)

Table (١) Comparison between the studied groups regarding mean area % of PAS:

	Mean ± SD %	Range %	F	p
Group I	93.72 ± 1.21	92.65 – 96.1		
Group II	94.88 ± 1.84	91.16 – 96.88	495.42	<0.001**
Group III	34.87 ± 5.83	29.14 – 48.69		
Group IV	77.22 ± 4.97	68.16 – 82.53		
posthoc	I-III <0.001**	I-II 0.915	I-IV <0.001**	
	II-III <0.001**	III-IV <0.001**		
	II-IV <0.001**			

F One way ANOVA test **p≤0.001 is statistically highly significant

Table (2) Comparison between the studied groups regarding mean area % of Caspase 3:

	Mean ± SD %	Range %	F	p
Group I	5.33 ± 1.52	3.14 – 7.43		
Group II	4.82 ± 0.78	3.61 – 5.8	1916.23	<0.001**
Group III	69.03 ± 3.86	59.5 – 71.77		
Group IV	11.16 ± 1.55	8.87 – 13.89		
posthoc	I-III <0.001**	I-II 0.957	I-IV <0.001**	
	II-III <0.001**	III-IV <0.001**		
	II-IV <0.001**			

F One way ANOVA test **p≤0.001 is statistically highly significant

Discussion:

Due to the near-daily household application of chlorpyrifos (CPF) for pest control (flies, cockroaches, ants) and its agricultural usage, CPF acts as an environmental contaminant with potential human health risks [(14)]. CPF has been documented to disrupt endocrine function and induce oxidative stress within the thyroid gland [(15)].

The current study aimed to evaluate histological, immunohistochemical, and ultrastructural alterations in the thyroid gland following six-week CPF exposure, as well as to investigate the potential protective effect of avocado oil when co-administered with CPF in adult male albino rats.

In this study, the control group (G I) and the avocado-treated group (G II) exhibited comparable histological, immunohistochemical, electron microscopic, and morphometric features; therefore, they were treated as equivalent for analytical purposes.

Examination of Hematoxylin and Eosin (H&E)-stained sections from the CPF-treated group (G III) revealed marked disruption of normal thyroid architecture. Follicles appeared degenerated and frequently fused. Colloid content was reduced or absent in many follicles. Follicular epithelial cells demonstrated hyperplasia, cytoplasmic vacuolization, nuclear pyknosis, desquamation into follicular lumina, and degenerative changes. Interfollicular connective tissue was expanded, with dilated and congested capillaries. Similar observations were reported previously [(16)]. These findings aligned with those of [(17)], who described H&E-stained thyroid sections exhibiting irregular follicles, desquamated luminal cells, absent colloid, fused follicles, obliterated lumina, and increased interfollicular cell populations.

Follicular fusion likely arises from membrane damage in epithelial cells. CPF's hydrophobic properties facilitate binding to phospholipid bilayers, inducing lipid peroxidation (LPO), a key mechanism of membrane injury. Consequently, adhesion to the basement membrane decreases, promoting epithelial desquamation. LPO promotes malondialdehyde (MDA) formation, serving as an oxidative stress marker and causing DNA and protein damage, thereby contributing to histopathological alterations [(18)]. CPF exposure increases reactive oxygen species (ROS), tumor necrosis factor-α (TNF-α), and interferon-γ (IFN-γ), further enhancing oxidative stress and inflammation. Additionally, CPF reduces reduced glutathione levels and impairs catalase and superoxide dismutase activities [(20)] [(21)].

Hyperplastic follicular walls may represent a compensatory response to thyroid-stimulating hormone (TSH) hypersecretion, secondary to ROS-induced follicular cell injury, which diminishes T3 and T4 production [(22)]. LPO also disrupts vascular walls, leading to vessel dilation and congestion [(23)], potentially reflecting attempts to eliminate the toxicant [(19)].

Periodic Acid-Schiff (PAS) staining of CPF-treated sections corroborated prior findings: weak PAS reactions were observed in colloid, with some follicles entirely empty, and the distorted basement membrane exhibited attenuated PAS positivity. Morphometric analysis confirmed a highly significant reduction ($P \leq 0.001$) in the area percentage of PAS-positive reaction in G III compared to G I. These results were consistent with [16], who reported weak PAS activity in basal lamina and moderate reaction in colloid of CPF-exposed follicles. Similarly, [17] documented negative PAS reactions in colloid and vacuolated follicular cells.

Immunohistochemical evaluation demonstrated strong nuclear and/or cytoplasmic caspase-3 immunoreactivity in many follicular cells of CPF-treated rats, with a highly significant increase in mean area percentage ($P \leq 0.001$) relative to controls. CPF accelerates follicular apoptosis via caspase-3, a crucial protease in self-activating apoptosis. Mitochondrial cytochrome c release triggered by ROS can further activate caspase-3 [24]. Apoptosis inhibitors may be deficient due to protein synthesis disturbances, contributing to cellular degeneration [25]. Pyroptosis, mediated by the NLRP3/Caspase-1 pathway, also plays a role in CPF-induced thyroid damage linked to oxidative stress [26].Previous studies showed that CPF increases pyroptosis-related protein expression, promoting inflammatory responses and oxidative stress through suppression of the Nrf2/Keap1 antioxidative pathway, with TNF-α and IL-1β contributing to apoptosis [27].

Transmission electron microscopy (TEM) of CPF-exposed thyroids revealed fused follicular epithelial cells, distorted apical microvilli, shrunken heterochromatic nuclei, cytoplasmic vacuolization, dilated rough endoplasmic reticulum, disrupted mitochondria, and numerous electron-dense lysosomes. Basement membranes appeared distorted. These findings were mirror to those of [24], who observed heterochromatic nuclei, dilated rough ER, vacuoles, and sparse apical microvilli in CPF-exposed follicles. ER dilatation may result from abnormal protein retention or imbalance between secretory product synthesis and removal [25]. Swollen organelles, including Golgi apparatus, ER, and mitochondria, contribute to intracytoplasmic vacuoles [28].

Avocado oil was employed for its high content of antioxidants, including tocopherols, phytosterols, carotenoids, and phosphatidylcholines (PCs), which mitigate CPF-induced oxidative damage [29]. In the CPF + avocado group (G IV), H&E sections demonstrated near-normal thyroid histology, with only a few follicles exhibiting degenerative changes, reduced colloid, and epithelial desquamation. These results corresponded with [16], who reported preserved glandular architecture following concomitant avocado pulp extract and CPF administration, with minor focal epithelial disruptions and dilated capillaries.

PAS staining in G IV confirmed these findings, showing moderate colloid reaction and weak basement membrane positivity, with a significant increase in area percentage of PAS-positive reaction ($P \leq 0.001$) relative to CPF alone. These observations were consistent with [16].

Caspase-3 immunoreactivity in G IV was negative in some cells and positive in others, with a highly significant reduction ($P \leq 0.001$) in mean area percentage compared to CPF alone. These results were in accordance with those of [16] who observed moderate positive caspase-3 immunoreactivity in the nuclei and/or the cytoplasm of few follicular cells. Avocado oil attenuated apoptosis via selective inhibition of caspase-3 [30].

TEM of G IV revealed restored follicular epithelial cells, intact apical microvilli, distinct cell membranes, euchromatic nuclei, and cytoplasm containing dilated rough ER and electron-dense lysosomes. A Previous research [31] demonstrated that

oral avocado oil enhances antioxidant enzyme activities (glutathione peroxidase, SOD, haem oxygenase-1, catalase) while decreasing MDA levels in a dose-dependent manner, highlighting its potent antioxidative capacity. Hydrophilic bioactive compounds, such as phenolics, may scavenge ROS and chelate transition metals, further protecting tissues [(32)].

Conclusion:

Avocado oil exerts a potent protective effect against CPF-induced thyroid damage, mitigating histological, histochemical, immunohistochemical, and ultrastructural alterations.

References

(1) Gilbert ME, Rovet J, Chen Z, Koibuchi N. Developmental thyroid hormone disruption: prevalence, environmental contaminants and neurodevelopmental consequences. Neurotoxicology. 2012 Aug 1; 33(4):842-52.

(2) Perry J, Cotton J, Rahman MA, Brumby SA. Organophosphate exposure and the chronic effects on farmers: a narrative review. Rural and Remote Health. 2020 Mar; 20(1):206-22.

(3) George N, Chauhan PS, Sondhi S, Saini S, Puri N, Gupta N. Biodegradation and analytical methods for detection of organophosphorous pesticide: chlorpyrifos. International Journal of Pure and Applied Sciences and Technology. 2014 Feb 1; 20(2):79.

(4) Mackay D, Giesy JP, Solomon KR. Fate in the environment and long-range atmospheric transport of the organophosphorus insecticide, chlorpyrifos and its oxon. Ecological risk assessment for chlorpyrifos in terrestrial and aquatic systems in the United States. 2014 Mar 12:35-76.

(5) Bernal-Rey DL, Cantera CG, dos Santos Afonso M, Menéndez-Helman RJ. Seasonal variations in the dose-response relationship of acetylcholinesterase activity in freshwater fish exposed to chlorpyrifos and glyphosate. Ecotoxicology and Environmental Safety. 2020 Jan 15; 187: 109673.

(6) Shiyovich A, Matot R, Elyagon S, Liel-Cohen N, Rosman Y, Shrot S et al. QT prolongation as an isolated long-term cardiac manifestation of dichlorvos organophosphate poisoning in rats. Cardiovascular Toxicology. 2018 Feb; 18(1):24-32.

(7) Flores M, Saravia C, Vergara CE, Avila F, Valdés H, Ortiz-Viedma J. Avocado oil: Characteristics, properties, and applications. Molecules. 2019 Jun 10; 24(11):2172.

(8) Pérez-Saucedo MR, Jiménez-Ruiz EI, Rodríguez-Carpena JG, Ragazzo-Sánchez JA, Ulloa JA, Ramírez-Ramírez JC et al. Properties of the avocado oil extracted using centrifugation and ultrasound-assisted methods. Food Science and Biotechnology. 2021 Aug; 30(8):1051-61.

(9) Krist S. Avocado oil. InVegetable fats and oils 2020 May 16 (pp. 87-93). Cham: Springer International Publishing.

(10) Krumreich FD, Prietsch LP, Antunes MD, Jansen-Alves C, Mendonça CR, Borges CD et al. Avocado oil incorporated in ultrafine zein fibers by electrospinning. Food Biophysics. 2019 Dec; 14(4):383-92.

(11) Chaudhary P, Khamar J, Sen DJ. Avocado: the holistic source as a natural doctor. World Journal of Pharmaceutical Research. 2015 May 12; 4(8):748-61.

(12) El-Sheikh AA, Ibrahim HM. The propolis effect on chlorpyrifos induced thyroid toxicity in male albino rats. Journal of Medical Toxicology and Clinical Forensic Medicine. 2017; 3(1):1-0.

(13) Ortiz-Avila O, Esquivel-Martínez M, Olmos-Orizaba BE, Saavedra-Molina A, Rodriguez-Orozco AR, Cortés-Rojo C. Avocado oil improves mitochondrial function and decreases oxidative stress in brain of diabetic rats. Journal of Diabetes Research. 2015; 2015(1):485759.

(14) Foong SY, Ma NL, Lam SS, Peng W, Low F, Lee BH et al. A recent global review of hazardous chlorpyrifos pesticide in fruit and vegetables: Prevalence, remediation and actions needed. Journal of hazardous materials. 2020 Dec 5; 400:123006.

(15) Ventura C, Nieto MR, Bourguignon N, Lux-Lantos V, Rodriguez H, Cao G, R et al. Pesticide chlorpyrifos acts as an endocrine disruptor in adult rats causing changes in mammary gland and hormonal balance. The Journal of steroid biochemistry and molecular biology. 2016 Feb 1; 156:1-9.

(16) Kassab AA, El-Aasr M. Effect of Avocado pulp extract on chlorpyrifos-induced thyroid gland injury in rats: A histological and morphometric study. Egyptian Journal of histology. 2018 Mar 1; 41(1):83-92.

(17) El-Kerdasy HI, Elsayed AM, Mousa HR. Ameliorative effect of ginger extract and selenium in theThyroid gland toxicity induced by chlorpyrifos in male albino rats. The Egyptian Journal of Hospital Medicine. 2021 Apr 1; 83(1):824-30.

(18) Manvitha V, Reddy AG, Kumar BA, Jeevanalatha M, Priyanka G. Protective Role of Ashwagandha and Selenium against

Chlorpyrifos (CPF) Induced Haemato-Biochemical and Hepatic Alterations in Wistar Rats. Int. J. Curr. Microbiol. App. Sci. 2019; 8(11):941-9.

(19) Hamid S. Histopathological effects of pesticide-cholopyrifos on kidney in albino rats. International Journal of Research in Medical Sciences. 2013 Oct; 1(4):465.

(20) Zhang Q, Zheng S, Wang S, Wang W, Xing H, Xu S. Chlorpyrifos induced oxidative stress to promote apoptosis and autophagy through the regulation of miR-19a-AMPK axis in common carp. Fish & shellfish immunology. 2019 Oct 1; 93:1093-9.

(21) Singh S, Kaur S, Budhiraja RD. Chlorpyrifos-induced oxidative stress in rat's brain and protective effect of grape seed extract. The Journal of Phytopharmacology. 2013; 2(3):26-33.

(22) Elwakeel EE, Zaki A. Histological and immunohistochemical alterations of thyroid gland after exposure to low frequency electromagnetic fields and protective effect of Vitamin C in adult male albino rat. J Am Sci. 2019;15: 56-64.

(23) Shady AM, FI NE. Effect of chlorpyrifos on thyroid gland of adult male albino rats. Egypt J Histol. 2010; 33(3):441-50.

(24) Abdelfadeel K, Mohamed M, Abd Elbaki B. Evaluation of the protective role of montelukast against the toxic effects of chloropyrifos on thyroid gland of adult male albino rats (A histological and immunohistochemical study). Journal of Medical Histology. 2023 Jun 1; 7(1):113-31.

(25) Rajkovic V, Matavulj M, Johansson O. Light and electron microscopic study of the thyroid gland in rats exposed to power-frequency electromagnetic fields. Journal of experimental biology. 2006 Sep 1; 209(17):3322-8.

(26) Bertheloot D, Latz E, Franklin BS. Necroptosis, pyroptosis and apoptosis: an intricate game of cell death. Cellular & molecular immunology. 2021 May; 18(5):1106-21.

(27) Gu B, Chen Y, Xu H, Zhan K, Zhu K, Luo H et al. Subchronic Chlorpyrifos Exposure Induces Thyroid Follicular Cell Pyroptosis to Exacerbate Thyroid Toxicity by Modulating Nrf2/Keap1/NF-κB Pathway in Male Mice. Journal of Inflammation Research. 2025 Dec 31:9307-20.

(28) Cavaletti G, Gilardini A, Canta A, Rigamonti L, Rodriguez-Menendez V, Ceresa C et al. Bortezomib-induced peripheral neurotoxicity: a neurophysiological and pathological study in the rat. Experimental neurology. 2007 Mar 1; 204(1):317-25.

(29) Tan CX, Chong GH, Hamzah H, Ghazali HM. Characterization of virgin avocado oil obtained via advanced green techniques. European Journal of Lipid Science and Technology. 2018 Oct; 120(10):1800170.

(30) Hamouda AF. Study on the effect of avocado on apoptosis, oxidative stress and injuries induced by diethyl nitrosamine in rat liver. Journal of Pharmacy and Pharmacology. 2015; 3(5):243-52.

(31) Tahsin A, Arif Muhammed R, Bayrakdarc E, Uthirapathy S. In-vitro antioxidant activity of avocado fruit oil in erbil, kurdistan region. Eurasian Journal of Science and Engineering. 2023; 8(3).

(32) Yamagata K. Endothelial protective effects of dietary phytochemicals: Focus on polyphenols and carotenoids. Studies in natural products chemistry. 2018 Jan 1; 55:323-50.

To cite this article: Nehal H. Mostafa , Essam M. Eid, Ali M. Ali, Marim F. Abdow. The Possible Protective Role of Avocado Oil on the Chlorpyrifos Pesticide Induced Thyroid Injury in Adult Male Albino Rats. (Light, Electron Microscopic and Immunohistochemical Studies). BMFJ XXX, DOI: 10.21608/bmfj.2026.428540.2694.